

# Nanoscale

Accepted Manuscript



This is an *Accepted Manuscript*, which has been through the Royal Society of Chemistry peer review process and has been accepted for publication.

*Accepted Manuscripts* are published online shortly after acceptance, before technical editing, formatting and proof reading. Using this free service, authors can make their results available to the community, in citable form, before we publish the edited article. We will replace this *Accepted Manuscript* with the edited and formatted *Advance Article* as soon as it is available.

You can find more information about *Accepted Manuscripts* in the [Information for Authors](#).

Please note that technical editing may introduce minor changes to the text and/or graphics, which may alter content. The journal's standard [Terms & Conditions](#) and the [Ethical guidelines](#) still apply. In no event shall the Royal Society of Chemistry be held responsible for any errors or omissions in this *Accepted Manuscript* or any consequences arising from the use of any information it contains.

1  
2  
3  
4  
5

6 Intracellular degradation of chemically functionalized carbon  
7 nanotubes using a long-term primary microglial culture model

8  
9

10 Cyrill Bussy<sup>1</sup>, Caroline Hadad<sup>2</sup>, Maurizio Prato<sup>2</sup>, Alberto Bianco<sup>3</sup> and Kostas Kostarelos<sup>1</sup>

11  
12  
13  
14  
15  
16  
17

<sup>1</sup> *Nanomedicine Lab, Faculty of Biology, Medicine and Health & National Graphene Institute, University of Manchester, AV Hill Building, Manchester M13 9PT, U.K.; Faculty of Life Sciences, University College London, Brunswick Square, London WC1N 1AX, U.K.*

<sup>2</sup> *Center of Excellence for Nanostructured Materials, Department of Chemical and Pharmaceutical Sciences, University of Trieste, Trieste, Italy*

<sup>3</sup> *CNRS, Institut de Biologie Moléculaire et Cellulaire, UPR 3572, Immunopathologie et Chimie Thérapeutique, Strasbourg, France*

18  
19  
20  
21  
22  
23  
24  
25  
26  
27  
28

**Abstract**

Chemically functionalized carbon nanotubes (*f*-CNTs) have been used in proof-of-concept studies to alleviate debilitating neurological conditions. Previous *in vivo* observations in brain tissue have suggested that microglia – acting as resident macrophages of the brain – play a critical role in the internalization of *f*-CNTs and their partial *in situ* biodegradation following a stereotactic administration in the cortex. At the same time, several reports have indicated that immune cells such as neutrophils, eosinophils and even macrophages could participate in the processing of carbon nanomaterials via oxidation processes leading to degradation, with surface properties acting as modulators of CNT biodegradability. In this study we questioned whether degradability of *f*-CNTs within microglia could be modulated depending on the type of surface functionalization used. We investigated the kinetics of degradation of multi-walled carbon nanotubes (MWNTs) functionalized via different chemical strategies that were internalized within isolated primary microglia over three months. A cellular model of rat primary microglia that can be maintained in cell culture for a long period of time was first developed. The Raman structural signature of the internalized *f*-CNTs was then studied directly in cells over a period of up to three months, following a single exposure to a non-cytotoxic concentration of three different *f*-CNTs (carboxylated, aminated and both carboxylated and aminated). Structural modifications suggesting partial but continuous degradation were observed for all nanotubes irrespective of their surface functionalization. Carboxylation was shown to promote more pronounced structural changes inside microglia over the first two weeks of the study.

**Key words**

Carbon nanotubes, functionalization, biocompatibility; biodegradation; central nervous system; Raman;

## 1 Introduction

2  
3 Surface functionalization of CNTs able to alter the hydrophobic character of pristine  
4 materials and therefore allow their use under physiological conditions has been shown to also  
5 greatly enhance their overall biocompatibility compared to unmodified CNTs.<sup>1</sup> Chemically  
6 functionalized carbon nanotubes (*f*-CNTs) have been proposed for a broad range of biomedical  
7 applications<sup>2</sup>, including neurology. CNTs have been studied for their suitability as substrates for  
8 neurite outgrowth, as components in implants or electrodes, and as drug or gene delivery  
9 systems for brain disorders.<sup>3</sup>

10 Amine-functionalized single-walled CNTs, directly injected in mouse brain ventricles, were  
11 shown to reduce the impact of ischemia and inflammation and offer neuroprotective effects.<sup>4</sup> We  
12 have previously demonstrated that MWNTs covalently functionalized by 1, 3-dipolar cycloaddition  
13 reaction were able to carry Caspase 3 siRNA into neurons, in order to alleviate ischemia-induced  
14 damages in the motor cortex of animals.<sup>5</sup> In these studies, *f*-CNTs were directly administered into  
15 the brain (ventricles or parenchyma). It is crucial to better understand the interactions of *f*-CNTs  
16 with the resident brain cells and their fate after injection. In addition, determination of the  
17 physicochemical nanotube features (such as length or surface character) as determinants of  
18 these interactions are largely ignored. Recently, we have shown *in vivo* that MWNTs that were  
19 oxidized prior to being amino-functionalized were able to induce a sustained inflammatory  
20 response and glial cell activation in areas peripheral to the injection site, whereas amino-  
21 functionalized MWNTs were only eliciting local and transient responses under similar conditions.<sup>6</sup>  
22 This suggested that the type of surface functionalization is an important component of the cellular  
23 responses of the brain tissue to *f*-CNT exposure.

24 CNTs have been thought to be non-degradable materials under physiological conditions  
25 due to a strong and chemically inert  $sp^2$  graphitic structure. However, in the last few years,  
26 several *in vitro* and *in vivo* reports have shown that CNTs can undergo an oxidation-mediated  
27 biodegradation under specific conditions present in responsive immune cells.<sup>7</sup> These findings  
28 indicated that biodegradation of carbon nanomaterials may require inflammation and the  
29 generation of reactive oxygen species to take place.<sup>8,9</sup> In addition, carbon nanomaterials bearing  
30 oxygenated groups (i.e. hydroxyl, carbonyl, carboxyl functions) were proven to be more  
31 degradable than carbon nanomaterials that have no or limited amount of oxygenated functions on  
32 their surface showing again the importance of surface chemistry.<sup>10-12</sup> Based on those studies, the  
33 concept of degradation-by-design was experimentally confirmed.<sup>13</sup> In this study, carbon nanotube  
34 surface was chemically modified to enhance the enzyme mediated degradation of the nanotubes.  
35 With regards to central nervous system (CNS), we have recently demonstrated that amino-  
36 functionalized MWNTs were undergoing structural deformations leading to partial degradation  
37 even two days after stereotactic injection into the mouse brain cortex, and that this degradation  
38 process was taking place in microglia.<sup>14</sup> An alteration of the graphitic structure of oxidized  
39 MWNTs suggesting intracellular processing was also observed after a short period of time (24-  
40 72h) in immortalized N9 microglial cells.<sup>15</sup> Nevertheless, knowledge on *f*-CNT degradation  
41 following cellular internalization within microglial cells remains limited and requires further  
42 investigations in particular to reveal the degradation kinetics and the physicochemical  
43 determinants of *f*-CNT degradability in the brain. Taken into account the important role of surface  
44 properties in terms of cell responses and biodegradability of carbon nanomaterials, we  
45 hypothesized that microglia-mediated degradation of *f*-CNTs will vary with the type of surface  
46 functionalization.

47 In this study, three different types of covalently functionalized *f*-MWNTs were used and  
48 the structural evolution of the internalized materials within primary microglial cells isolated from

1 rat embryonic brain was directly assessed via Raman spectroscopy, a sample preparation- free  
2 technique, at different time points over 3 months. The aim of this study was to investigate *in situ*  
3 whether the type of surface functionalization influenced the degradability of *f*-MWNTs, and to  
4 describe the kinetics of degradation in a primary cellular model in the long-term using long-lasting  
5 non-dividing cells. We report that isolated primary microglia have the ability to internalize, contain  
6 and continuously degrade over time various *f*-CNTs irrespective of their surface functionalization,  
7 although carboxylation allowed faster structural deformation in the first two weeks of the study.  
8 Notably, *f*-MWNTs were still present in the primary microglial cells even 3 months after their initial  
9 internalization, suggesting that microglia can store *f*-CNTs for a long period of time without  
10 apparent damages, and that degradation in isolated microglia can occur in a slow but continuous  
11 process.

## 12 13 14 **Results and Discussion**

15  
16 **Chemical structure and characterisation of MWNT suspension.** Three different chemically  
17 functionalized MWNTs were synthesized from the same batch of pristine starting material to  
18 eliminate variations in the content of metal (or other) impurities. **Figure 1a** shows the chemical  
19 structure of the *f*-MWNTs studied that included: (i) carboxylated MWNTs (ox-MWNTs) prepared  
20 by treatment in strong acid conditions;<sup>16</sup> (ii) amino-functionalized oxidised MWNTs (ox-MWNT-  
21  $\text{NH}_3^+$ ) prepared by 1,3 dipolar-cycloaddition reaction after their initial oxidation as previously  
22 described, hence both ox-MWNTs and ox-MWNT- $\text{NH}_3^+$  have the same amount of carboxylic  
23 functions;<sup>14</sup> and (iii) amino-functionalized MWNTs (MWNT- $\text{NH}_3^+$ ) prepared following the 1,3  
24 dipolar-cycloaddition reaction on pristine MWNTs as previously reported.<sup>17, 18</sup> Functionalized  
25 MWNTs that have undergone oxidation are shorter (200-300 nm in length for ox-MWNT and ox-  
26 MWNT- $\text{NH}_3^+$ ) than the *f*-MWNTs without initial oxidation (i.e. MWNT- $\text{NH}_3^+$ ) which kept a similar  
27 length as the pristine starting material (between 0.5-2  $\mu\text{m}$ ).

28 The degree of amino group loading on the side walls and tips of the *f*-MWNTs as  
29 determined by the Kaiser test is summarized in **Figure 1b**. All MWNT suspensions were  
30 prepared in 5% dextrose using bath sonication and they exhibited good aqueous dispersibility  
31 prior to their incubation within cells. The Raman spectroscopy analysis of the different *f*-MWNT  
32 suspensions revealed the characteristic peak at 1330  $\text{cm}^{-1}$  (D band), 1585  $\text{cm}^{-1}$  (G band) and  
33 1620  $\text{cm}^{-1}$  (D' band) for all nanotubes (**Figure 1c**). Oxidation of nanotubes that introduced  
34 carboxyl groups in their graphitic lattice as well as shortening, also led to higher amount of  
35 structural defects as reflected by a more pronounced and intense D' band for both ox-MWNT and  
36 ox-MWNT- $\text{NH}_3^+$  compared to MWNT- $\text{NH}_3^+$  that was functionalized without prior oxidation (**Figure**  
37 **1c**). For MWNT- $\text{NH}_3^+$ , the D' band only appeared as a shoulder on the G band of the Raman  
38 spectra, suggesting a less defected structure compared to the other two materials. These results  
39 are in agreement with a previous report showing that oxidation could induce an increase of  
40 defects that can be assessed via Raman spectroscopy.<sup>19</sup>

41  
42 **Live imaging of primary microglia cell culture exposed to functionalized carbon**  
43 **nanotubes.** In previous studies, we have reported preferential internalization of *f*-MWNTs by  
44 microglia in primary co-culture<sup>20</sup> or following intra-parenchymal injection into the brain tissue<sup>5, 6</sup>  
45 and have also shown that microglia are involved in the *in vivo* partial degradation of amino-  
46 functionalized MWNTs.<sup>14</sup> It was also showed that agglomerates of oxidized MWNTs can be  
47 untangled, internalised and then intracellularly processed to some extent by immortalized N9

1 microglial cells.<sup>15</sup> However, the kinetics of degradation and physicochemical characteristics of the  
2 MWNTs responsible for the microglia-mediated degradation were not investigated. To address  
3 this, and in order to study continuously the biodegradation of carbon nanotubes in the long-term  
4 using a relevant *in vitro* model, we developed a specific model of primary microglia cell cultures.  
5 We reasoned that to mirror the *in vivo* brain tissue we needed non-dividing cells that can be  
6 maintained and monitored for a long period of time (i.e. few months) following a single exposure  
7 to nanotubes. This would allow monitoring the effects of cells on *f*-MWNTs measured by Raman  
8 spectroscopy at the same particular single cell level and would not be the result of successive cell  
9 divisions.

10 Based on our observations that after one passage, the microglia population was not  
11 expanding, we developed microglia-enriched cell cultures with a stable total cell population that  
12 could be maintained in 12% FBS completed medium for at least 3 months (with only a normal  
13 decrease of the initial population over time, about 30% compared to the initial cell number). In the  
14 brain, the define longevity of microglial cells is unknown, but it is widely acknowledged that as  
15 specialised tissue macrophages they have a long lifespan –possibly decades in humans- and  
16 divide only upon inflammatory activation.<sup>21, 22</sup> Here, the enriched microglia cell cultures were  
17 obtained after mild trypsination<sup>23</sup> of mixed glial cell cultures isolated from foetal rat brain. Two  
18 days after mild trypsination, isolated microglia were exposed for 24h to 10µg/mL of *f*-MWNT  
19 suspensions. This dose was shown previously to be non-toxic for isolated microglia.<sup>20</sup> The next  
20 day, *f*-MWNTs present in the supernatant were removed and the cell monolayers were from that  
21 point maintained in MWNT-free cell culture conditions for various periods of time until Raman  
22 analysis.

23 The timeline of exposure and recovery periods are shown in **Figure 2a**. The microscopic  
24 aspect of live microglia cells following *f*-MWNT exposure are also reported for different time  
25 points after exposure (**Figure 2b**). Optical microscopy images of the exposed cells (live imaging)  
26 revealed that microglia internalised a large amount of *f*-MWNTs irrespective of their surface  
27 functionalization. Typically, *f*-MWNTs appearing as black material accumulated in the perinuclear  
28 region probably in phagolysosomes as suggested by the granular aspect of the perinuclear  
29 accumulation (for higher magnification see **Figure S1**). The nanotube-loaded vesicles filled  
30 almost the whole cytosol, even masking the nucleus when microglial cells were round shaped.  
31 Only the nucleus, the extremities and the external boundaries of the cells appeared as clear  
32 regions free of *f*-MWNTs when comparing phase contrast images versus bright field images for  
33 the same observation field (**Figure S1**). As a function of time, no significant differences were  
34 observed in the lightening of the darker regions in cells, or between the different *f*-MWNTs. This  
35 suggested that degradation, if happening, was not complete and did not lead to cells appearing  
36 devoid of any material. In addition, there was no difference in terms of shape or number of cells  
37 between the different exposures and in comparison to non-exposed cells, indicating that the  
38 concentration selected was not affecting cell morphology or viability. Cell morphology is a good  
39 indicator of cell response to toxic agents, especially for macrophages and microglia (that act as  
40 resident macrophages of the CNS). When macrophages are activated, they usually change their  
41 morphology compared to their initial shape. Throughout these experiments, cells exhibited the  
42 same normal shape as previously reported.<sup>20, 23</sup>

43 **Raman spectroscopy of primary microglia cell culture exposed to functionalized carbon**  
44 **nanotubes.** While TEM and XPS analyses of CNTs following intracellular degradation would be  
45 greatly helpful to assess respectively the extent of structural alteration<sup>9, 24</sup> and the evolution of  
46 surface chemistry, they would both require multiple careful steps of extraction and purification in  
47 order to avoid introduction of further damages not due to biodegradation and to get access to the

1 CNT surfaces and diameters after their internalisation and intracellular degradative processing.  
2 To address the question of the kinetic in the long term, we therefore decided to use a non-  
3 destructive and sample preparation-free technique, Raman spectroscopy, which would allow  
4 interrogating the structure integrity of CNTs *in situ* without any alteration due to sample  
5 processing procedures.

6 Following the 24 h exposure to different *f*-MWNTs and a period of recovery from 1 day to 90  
7 days, the microglia cell cultures were washed with PBS (without calcium and magnesium) and  
8 then fixed with methanol, in order to minimise the noise on the Raman scattering signal coming  
9 from the cell background. Raman spectroscopy was then performed at a single cell level, using  
10 the 100x objective of the microscope in order to access the different compartments of a cell  
11 (nucleus, cytosol, extremities). Cells were randomly selected over the whole surface of the glass  
12 coverslip used as support for the microglia culture. Depending on cell surface, between 12 and  
13 22 spots were selected for Raman spectroscopy analysis within each single cell, as illustrated in  
14 **Figure 3**. In agreement with the live imaging of microglia (**Figure 2**), no difference was observed  
15 between the different MWNT exposures or over time in terms of cytoplasmic MWNT loading,  
16 while the nucleus appeared clear of any material.

17 Raman analysis performed in the nuclear region confirmed that no *f*-MWNTs were accumulated  
18 in that region irrespective of the *f*-MWNTs or the time of recovery considered (data not shown).  
19 When Raman spectroscopy was performed in cell regions with the presence of large amounts of  
20 dark material, the characteristic peaks of MWNTs (mainly D and G bands, with D' band on the  
21 side of G band) were obtained for all the *f*-MWNT exposed cells for the duration of the experiment  
22 (**Table S1**). This suggested that nanotube degradation was not complete, even after 90 days of  
23 residency inside microglia, thus confirming our initial optical microscopic observations. These  
24 findings are in agreement with many reports showing that MWNTs are carbon nanostructures  
25 with a lower degree of degradability compared to SWCNTs or graphene-related materials, mainly  
26 attributed to their multi-layered architecture.<sup>9, 25</sup> Multi-layered tubes arranged in a concentric  
27 manner are likely less degradable than carbon materials consisting of one single layer.

28 In order to better understand whether the structure of the *f*-MWNTs have been modified during  
29 the period of residency inside the microglia, we calculated the intensity ratio of the D over G  
30 bands that is a known indicator of structural modifications and degree of defects. **Figure 4** shows  
31 the evolution of the  $I_D/I_G$  ratios (and  $I_D/I_G$  means) for the different *f*-MWNTs over time. Structural  
32 modifications evidenced by an overall decrease of the mean  $I_D/I_G$  ratios from day 1 to 90 were  
33 found for all three types of nanotubes (1.95±0.10 to 1.70±0.17 for ox-MWNTs; 2.12±0.10 to  
34 1.87±0.13 for ox-MWNT-NH<sub>3</sub><sup>+</sup>; and 1.65±0.15 to 1.49±0.15 for MWNT-NH<sub>3</sub><sup>+</sup>). This suggested that  
35 a degradative process for all the three types of *f*-MWNTs was taking place within microglia  
36 leading to an accumulation of structural defects. Interestingly, the evolution of  $I_D/I_G$  ratios over  
37 time was different between the three types of functionalized nanotubes with an initial phase of 15  
38 days during which oxidised nanotubes (ox-MWNTs and ox-MWNT-NH<sub>3</sub><sup>+</sup>) exhibited a more rapid  
39 pattern of degradation compared to non-oxidised nanotubes (MWNT-NH<sub>3</sub><sup>+</sup>), followed by a second  
40 phase during which all three nanotubes seemed to undergo further structural deformation but at a  
41 similar rate.

42 For materials bearing free carboxylic functions (ox-MWNTs and ox-MWNT-NH<sub>3</sub><sup>+</sup>), evolution of the  
43  $I_D/I_G$  ratios between consecutive time points was more significant during the first two weeks after  
44 exposure, as evidenced by continuous decrease of the ratio during that period, but was slowing  
45 down thereafter with even an increase of the band ratio at 30 and 60 days before decreasing  
46 again at 90 days. Materials functionalized with the 1,3-dipolar cycloaddition reaction (MWNT-

1 NH<sub>3</sub><sup>+</sup>) also underwent structural modifications from day 1 to 90, but differences in band ratio  
2 between consecutive time points were slightly less pronounced than for carboxylated materials  
3 during the first two weeks. However, as for oxidized nanotubes, evolution of I<sub>D</sub>/I<sub>G</sub> ratios at later  
4 time points was characterized by alternation of decreasing and increasing levels. These  
5 observations suggested that all *f*-MWNTs degraded over time in microglia in a non-linear fashion  
6 and that the rate and kinetic of degradation of MWNT-NH<sub>3</sub><sup>+</sup> was different from the ones of  
7 oxidized nanotubes. The initial presence of higher amount of structural defects on the surface of  
8 carboxylated materials, evidenced in Raman spectra by the presence of higher D' band and due  
9 to post-synthesis acidic treatment (**Figure 1**), could explain the higher rate of degradation  
10 observed for these materials during the first 14 days compared to non-oxidized nanotubes.  
11 Comparisons between oxidized with non-oxidized material (or material with limited amount of  
12 oxidation) have shown that a highest degree of degradation is always associated with oxidized  
13 nanostructures.<sup>7, 10-12, 15, 26, 27</sup> Presumably, the initial structural defects due to oxidation play the  
14 role of initiator sites for further structural modifications (via enzyme-catalyzed oxidation  
15 processes) leading to higher degradation over time.<sup>10, 28</sup> The most defected materials will  
16 therefore undergo the highest structural alteration.

17 A non-linear pattern of structural modifications over time was observed in the present study  
18 (sequential increase and decrease of the I<sub>D</sub>/I<sub>G</sub> band ratio, **Figure 4**). This was interpreted as the  
19 alternation between two types of previously reported processes. In the first case, evidenced by a  
20 decrease of the I<sub>D</sub>/I<sub>G</sub> band ratio, degradation of CNTs by a defect-consuming process was taking  
21 place, whereby defects disappeared with time due to the removal of the damaged parts of the  
22 tubes.<sup>29</sup> In the case of functionalized MWNTs, these damaged parts would be primarily the outer  
23 walls, not only the functional groups or the outermost layer bearing the functional groups but also  
24 the first few outer layers that have been defected due to the functionalization chemical  
25 procedures. Therefore, in the present study and amongst the 3 CNTs tested, the fastest to  
26 degrade CNTs would be the two types of carboxylated CNTs (ox-MWNTs, ox-MWNT-NH<sub>3</sub><sup>+</sup>) that  
27 bear significant surface defects due to the oxidation reaction. Layers underneath the oxidized  
28 ones would be expected to be more resistant to biodegradation, due to less oxidation defects and  
29 a structure close to pristine. This hypothesis is consistent with the results reported here, where a  
30 sharp degradation for the two carboxylated CNTs was observed over the first two weeks (i.e.  
31 degradation of the few outermost defected layers), followed by a much slower degradation  
32 pattern over time (i.e. of the remaining deeper layers that are significantly less defected). In the  
33 second type of degradation processes previously reported, more defects appeared on the surface  
34 (in addition to the pre-existing ones) due to enzyme-catalyzed oxidation leading to an increase of  
35 the ratio, mainly attributed to higher D band intensity.<sup>25, 30, 31</sup> In agreement with the latter  
36 statement, when Raman spectroscopy was performed on microglia exposed to MWNT-NH<sub>3</sub><sup>+</sup> at  
37 30, 60 and 90 days, we observed in some cases the appearance of a clear D' band in correlation  
38 with an increase of the D peak intensity also known as indication of higher structural defects, as  
39 shown in **Figure 5**. Considering that the starting MWNT-NH<sub>3</sub><sup>+</sup> materials did not display a clear D'  
40 band (**Figure 1**), this suggested that MWNT-NH<sub>3</sub><sup>+</sup> were undergoing degradation via a defect-  
41 accumulating process, possibly oxidation via reactive oxygen species as reported previously.<sup>9</sup>  
42 In order to prove or dispute any of these working hypotheses of degradation mechanisms, specific  
43 further experiments will be required. For instance, studies addressing the evolution of CNT  
44 diameters over time using TEM would help to reveal the real mechanisms at stake and to  
45 compare to previous studies.<sup>7, 24, 32</sup> But this was not in the scope of the present study focusing on  
46 the kinetic of degradation in the long term.

1 Although carbon nanostructures have been assumed resilient due to their strong inert  $sp^2$   
2 hybridised carbon structure, their degradation under physiological conditions is now well  
3 acknowledged.<sup>8, 28, 33</sup> Since the first demonstration that SWCNTs,<sup>12, 34</sup> MWNTs<sup>10</sup> and graphene<sup>27,</sup>  
4<sup>35</sup> can all undergo oxidation-based degradation after incubation with peroxidases in the presence  
5 of  $H_2O_2$ , there have been numerous reports of such oxidation-mediated processes taking place  
6 both *in vitro* and *in vivo*. Immune cells involved in the pulmonary response to CNTs such as  
7 neutrophils and eosinophils were successively reported to be able to digest SWNTs, by the action  
8 of myeloperoxidase and eosinophil peroxidase respectively.<sup>32, 36</sup> It was then shown at the *in vivo*  
9 level that degradation of SWNTs via the myeloperoxidase-mediated oxidation process was  
10 occurring in the lungs of animals after pharyngeal aspiration.<sup>37</sup> In addition, carboxyl functionalized  
11 graphene was also shown to degrade over a period of 3 months in the resident macrophages of  
12 various tissues such as lung, liver, kidney and spleen.<sup>38</sup> After 3 months, the highest degree of  
13 degradation leading to amorphous carbon was documented in the spleen which is one of the  
14 major organs of the mononuclear phagocytic system.<sup>39</sup> With regards to brain, we have previously  
15 reported that microglia were the main cells responsible for the *in situ* internalisation and  
16 degradation of *f*-MWNTs injected directly in the cortical parenchyma.<sup>14</sup> In agreement with the  
17 results reported here, we observed an overall decrease of the  $I_D/I_G$  ratio over a period of 14 days  
18 for MWNT-NH<sub>3</sub><sup>+</sup> albeit to a different extent as *in vivo* degradation seemed to be a more dynamic  
19 process involving more cells (such as brain perivascular macrophages) and potentially clearance  
20 mechanisms than a static *in vitro* model of isolated microglia. While the exact biodegradation  
21 mechanism and kinetics remain here elusive and will require more in-depth *in vitro* investigations,  
22 we can foresee that *in vivo* studies will be required to fully understand the extent of degradability  
23 of carbon nanomaterials in the long term.

24 Biodegradation of carbon nanomaterials is seen as a way to eliminate carbon-based vector and  
25 therapeutic or diagnostic transport systems after achieving their function.<sup>33</sup> However,  
26 biodegradative processes should also be considered as potential determinants of the overall  
27 toxicological profile of nanomaterials due to the uncertain nature and impact of the degradation  
28 by-products.<sup>40</sup> Not only degradation can potentially lead to production of by-products of more  
29 acute cytotoxicity than the starting non-degraded material, but also can form transient  
30 nanostructures some of which may have shown higher toxicity. For example, one of the possible  
31 issues resulting from degradation of thicker MWNTs is the production of thinner MWNTs due to  
32 peeling/exfoliation of outer layers. Thinner MWNTs have been shown to pose a higher  
33 toxicological risk than thicker nanotubes.<sup>41, 42</sup> Reassuringly, two studies have shown that CNTs  
34 that degraded *in test tube* under specific conditions and then administered in animals did not  
35 induce any toxic effects. In the first study, biodegraded SWNTs administered by pharyngeal  
36 aspiration did not induce inflammatory responses.<sup>32</sup> In the second study, MWNTs shortened by a  
37 10-week long treatment in phagolysosome-mimicking solution did not produce any pathogenic  
38 effects after injection in the peritoneal cavity.<sup>43</sup> Amino functionalized MWNTs (via arylation)  
39 processed for 24hrs in THP-1 derived macrophages were also assessed for their cytotoxicity after  
40 extraction.<sup>9</sup> THP-1 processed MWNTs displaying holes in their walls were shown to be less toxic  
41 to THP-1 cells than the original (non-predigested) nanotubes. Similarly, in a previous study<sup>20</sup> or  
42 in the present study (**Figure 2a and 2b**) we did not observe any toxic or obvious deleterious  
43 effects on the microglial cells at the concentration used here (i.e. 10  $\mu\text{g/mL}$ ) even after 90 days.  
44 Since occurrence of degradation is confirmed over time, further experiments focusing on the  
45 microglial cell functionality at this non-toxic concentration will answer definitely to the question of  
46 possible damaging effects of the by-products.

1 Among all the studies of carbon nanostructure degradation that have been reported in the  
2 literature, surface properties have emerged as a determinant parameter of the rate of  
3 degradation. Degree of carboxylation was shown to directly impact on the ability of materials to  
4 degrade. Graphene oxide was shown to degrade after incubation with HRP and  
5 myeloperoxidase, whereas a reduced form of graphene oxide was unable to undergo degradation  
6 under similar conditions.<sup>27, 35</sup> Li *et al* confirmed those findings and also found that graphene oxide  
7 non-covalently functionalized with bovine serum albumin or PEG was resistant to HRP mediated  
8 oxidation.<sup>11</sup> They also suggested that the protein coating prevented the close interaction between  
9 the graphene oxide with the peroxidase, therefore limiting its further oxidation and degradation. In  
10 contrast, covalently PEGylated SWNTs were shown to degrade in various peroxidase containing  
11 solutions.<sup>44</sup> Interestingly, when graphene oxide was covalently PEGylated via a cleavable bond,  
12 when incubated under conditions that favoured bond cleavage, the released graphene oxide  
13 could undergo degradation in a similar manner as bare graphene oxide.<sup>11</sup> In another study, the  
14 amount of defects in the graphitic lattice of the carbon nanomaterials was also shown to be an  
15 important parameter, as evidence by a quicker degradation of nitrogen-doped MWNTs compared  
16 to oxidised MWNTs.<sup>10</sup> Such findings also demonstrate that degradability of carbon nanomaterials  
17 can be tailored by surface functionalization as some of us recently illustrated,<sup>13</sup> opening up the  
18 possibility to exciting future investigations of engineering degradability cues and effectors on the  
19 surface of the nanomaterial.

20

## 21 **Conclusions**

22

23 The present study reports the evolution over time of the Raman signature of different  
24 functionalized carbon nanotubes internalized inside primary microglia. The accumulating  
25 structural changes of intracellularly-localized carbon nanotubes were attributed to partial  
26 degradation of the materials inside cells that varied according to their initial type of surface  
27 functionalization. While surface carboxylation enhanced degradation during the first two weeks in  
28 comparison to amination, no difference in the rate and kinetics of degradation was then observed  
29 between carboxylation and amination. Irrespective of the type of chemical functionalization,  
30 partial degradation occurred for all types of nanotubes and was progressive over the timeline of  
31 the study (90 days). Overall it can be described as a slow but continuous process. These findings  
32 highlight the importance of surface chemical functionalization toward the development of carbon  
33 nanomaterials not only biocompatible but also with tailored biodegradability,<sup>13, 33</sup> in particular for  
34 biomedical applications in the CNS.

35

36

## 37 **Acknowledgments**

38 This work was supported by the European Commission, under the FP-7 *Marie Curie* actions,  
39 (Career Development Intra-European Fellowship, PIEF-GA-2010-276051, project  
40 NANONEUROHOP). AB wishes to thank the CNRS financial support from PICS (Project for  
41 International Scientific Cooperation). The authors also thank T. Bernard for her help during the  
42 analysis of the Raman data.

43

44

## 1 Experimental

2  
3 **Materials.** Multiwalled carbon nanotubes (MWNT) were purchased from Nanostructured and Amorphous  
4 Materials Inc. (Houston, TX, USA; Lot # 1240XH, 95%). The outer average diameter was 20-30 nm, and  
5 the length was 0.5-2  $\mu\text{m}$ . The chemicals and solvents were obtained from Sigma-Aldrich (UK). Cell culture  
6 reagents (PBS, trypsin, foetal bovine serum, DMEM:F12) were purchased from Gibco (Life technologies,  
7 UK). The different chemical functionalizations of multi-walled carbon nanotubes were performed following  
8 well-established procedures previously reported by our groups.<sup>16-18, 45, 46</sup> The amount of COOH after the  
9 oxidation reaction as been previously calculated using thermogravimetric analysis, corresponding to 1,7  
10  $\mu\text{mol/g}^{25}$ .

11  
12 **Preparation of MWNTs for cell exposure.** A 1 mg/mL stock suspension of functionalized MWNTs was  
13 prepared with sterile 5% dextrose in distilled water, sonicated 45 min and stored at  $-20^{\circ}\text{C}$  before further  
14 use. After thawing, the CNT suspension was sonicated 10 min before further dilution (10  $\mu\text{g/mL}$ ) in serum  
15 free cell culture medium. Sterile dextrose solution was used as control with cells non-exposed to CNTs; a  
16 0.05% dextrose solution (500  $\mu\text{g/mL}$ ) was prepared with serum free cell culture medium.

### 17 Primary cell cultures

18 **Primary mixed glial cell cultures.** Mixed glial cell cultures were prepared with striatum extracted from E16-  
19 E18 Wistar foetal rat brains (standard Witschi stages 33-34). Striatal tissue pieces were dissociated to  
20 single cell suspensions by trypsinisation followed by mechanical trituration in  $\text{Ca}^{2+}/\text{Mg}^{2+}$  free HBSS solution  
21 <sup>47, 48</sup>. After determination of the number of live cells, six millions of cells were plated onto poly-D-lysine (50  
22  $\mu\text{g/ml}$ ) coated 75  $\text{cm}^2$  flask with DMEM:F12 medium completed with 12% heat inactivated foetal bovine  
23 serum and incubated at  $37^{\circ}\text{C}$  in a humidified 5%  $\text{CO}_2$  incubator. Medium was changed daily for a 10 days  
24 period, after which the cell monolayer was trypsinised, splitted (2/3 ratio), and seeded onto 60 mm glass  
25 coverslips coated with poly-L-lysine (50  $\mu\text{g/ml}$ ) that were individually hosted in 6 well plates.

26  
27 **Primary microglia enriched cell cultures.** Microglia enriched cell cultures were prepared from striatal mixed  
28 glial cultures at passage 1, according to previously described method, based on mild trypsinisation.<sup>23</sup> At  
29 confluence, the cell monolayer on glass coverslip was treated with trypsin diluted in serum free DMEM:F12  
30 medium (final trypsin concentration 0.05%) until all cells detached, except microglial cells which remained  
31 attached to the glass coverslip. After washing with serum free DMEM:F12 medium, cells were cultured in  
32 DMEM:F12 medium completed with 12% heat inactivated foetal bovine serum. Cells obtained after this  
33 treatment were all positive for Ox42, a biomarker of microglia (data not shown). After 48 h incubation,  
34 microglia enriched cell cultures were treated with CNTs (10  $\mu\text{g/mL}$ ).

35  
36 **Exposure of microglial cells to functionalized MWNTs.** Microglia enriched cell cultures were first  
37 exposed for 2 h to a 10  $\mu\text{g/mL}$  CNT suspension prepared in serum free cell culture medium (DMEM:F12  
38 medium). After 2 h incubation at  $37^{\circ}\text{C}$  without serum, the cell culture medium was completed with heat  
39 inactivated foetal bovine serum (12%). After 24 h incubation at  $37^{\circ}\text{C}$ , the supernatant - still containing  
40 CNTs - was removed, cells were washed twice with PBS and then incubated with CNT free complete  
41 medium (DMEM:F12 with 12% serum) for 1, 7, 14, 30, 60 and 90 days (recovery period). CNT free  
42 complete medium was changed every 3 days. At the end of exposure, cells on glass coverslips were  
43 washed twice with PBS and then fixed with methanol, previously cooled at  $-20^{\circ}\text{C}$ , for 10 min at  $-20^{\circ}\text{C}$ . The  
44 glass coverslips were then removed from the well plates, air dried for at least 1 hour under the air flow of a  
45 microbiology safety cabinet, fixed on microscopy glass slide with nail polish, and stored in slide boxes at  
46 room temperature until further Raman analysis.

47  
48 **Raman spectroscopy.** Raman spectroscopic analyses were performed with a Thermo Scientific DXR  
49 Raman microscope, equipped with an Olympus microscope and a 633 nm LASER, using a 100x objective  
50 lens and 1 mW of LASER power. Each spectrum has been recorded on a specific spot area (1  $\mu\text{m}^2$ )  
51 randomly selected within the cell demarcations (see Figure 3 as example of spot map). Each spectrum  
52 recorded is the average of 3 times 50 s of LASER illumination for one spot. For each cell randomly selected  
53 within the cells covering the glass coverslip, between 12 and 22 spectra were recorded, depending on the  
54 cell surface. A minimum of 10 cells per samples (3 different CNTs and 6 different time points) have been  
55 analysed by Raman microscopy. Each spectrum were analysed individually to determine the highest  
56 intensity of the different characteristic peaks for CNTs, meaning G, D, D' and G' (2D) bands<sup>49-51</sup>. Raman  
57 spectra were corrected for cell auto-fluorescence (fluorescence coming from the cell and the glass support)  
58 and normalised to G band intensity ( $I_G=1$ ) so as to determine the  $I_D/I_G$  band ratio.

1

2 **References**

- 3 1. A. Battigelli, C. Menard-Moyon, T. Da Ros, M. Prato and A. Bianco, *Adv Drug Deliv Rev*, 2013, **65**, 1899-1920.
- 4 2. B. S. Wong, S. L. Yoong, A. Jagusiak, T. Panczyk, H. K. Ho, W. H. Ang and G. Pastorin, *Adv Drug Deliv Rev*, 2013,
- 5 **65**, 1964-2015.
- 6 3. A. Nunes, K. Al-Jamal, T. Nakajima, M. Hariz and K. Kostarelos, *Arch Toxicol*, 2012, **86**, 1009-1020.
- 7 4. H. J. Lee, J. Park, O. J. Yoon, H. W. Kim, Y. Lee do, H. Kim do, W. B. Lee, N. E. Lee, J. V. Bonventre and S. S.
- 8 Kim, *Nat Nanotechnol*, 2011, **6**, 121-125.
- 9 5. K. T. Al-Jamal, L. Gherardini, G. Bardi, A. Nunes, C. Guo, C. Bussy, M. A. Herrero, A. Bianco, M. Prato, K.
- 10 Kostarelos and T. Pizzorusso, *Proc Natl Acad Sci U S A*, 2011, **108**, 10952-10957.
- 11 6. G. Bardi, A. Nunes, L. Gherardini, K. Bates, K. T. Al-Jamal, C. Gaillard, M. Prato, A. Bianco, T. Pizzorusso and K.
- 12 Kostarelos, *PLoS One*, 2013, **8**, e80964.
- 13 7. G. P. Kotchey, S. A. Hasan, A. A. Kapralov, S. H. Ha, K. Kim, A. A. Shvedova, V. E. Kagan and A. Star, *Acc Chem*
- 14 *Res*, 2012, **45**, 1770-1781.
- 15 8. K. Bhattacharya, F. T. Andon, R. El-Sayed and B. Fadeel, *Adv Drug Deliv Rev*, 2013, **65**, 2087-2097.
- 16 9. D. Elgrabli, W. Dachraoui, C. Menard-Moyon, X. J. Liu, D. Begin, S. Begin-Colin, A. Bianco, F. Gazeau and D.
- 17 Alloeyau, *ACS Nano*, 2015, **9**, 10113-10124.
- 18 10. Y. Zhao, B. L. Allen and A. Star, *J Phys Chem A*, 2011, **115**, 9536-9544.
- 19 11. Y. Li, L. Feng, X. Shi, X. Wang, Y. Yang, K. Yang, T. Liu, G. Yang and Z. Liu, *Small*, 2014, **10**, 1544-1554.
- 20 12. B. L. Allen, G. P. Kotchey, Y. Chen, N. V. Yanamala, J. Klein-Seetharaman, V. E. Kagan and A. Star, *J Am Chem*
- 21 *Soc*, 2009, **131**, 17194-17205.
- 22 13. A. R. Sureshbabu, R. Kurapati, J. Russier, C. Menard-Moyon, I. Bartolini, M. Meneghetti, K. Kostarelos and A.
- 23 Bianco, *Biomaterials*, 2015, **72**, 20-28.
- 24 14. A. Nunes, C. Bussy, L. Gherardini, M. Meneghetti, M. A. Herrero, A. Bianco, M. Prato, T. Pizzorusso, K. T. Al-Jamal
- 25 and K. Kostarelos, *Nanomedicine (Lond)*, 2012, **7**, 1485-1494.
- 26 15. A. E. Goode, D. A. Gonzalez Carter, M. Motskin, I. S. Pienaar, S. Chen, S. Hu, P. Ruenraroengsak, M. P. Ryan, M.
- 27 S. Shaffer, D. T. Dexter and A. E. Porter, *Biomaterials*, 2015, **70**, 57-70.
- 28 16. S. P. Li, W. Wu, S. Campidelli, V. Sarnatskaia, M. Prato, A. Tridon, A. Nikolaev, V. Nikolaev, A. Bianco and E.
- 29 Snezhkova, *Carbon*, 2008, **46**, 1091-1095.
- 30 17. V. Georgakilas, K. Kordatos, M. Prato, D. M. Guldi, M. Holzinger and A. Hirsch, *J Am Chem Soc*, 2002, **124**, 760-
- 31 761.
- 32 18. V. Georgakilas, N. Tagmatarchis, D. Pantarotto, A. Bianco, J. P. Briand and M. Prato, *Chem Commun (Camb)*,
- 33 2002, 3050-3051.
- 34 19. M. S. Dresselhaus, G. Dresselhaus, A. Jorio, A. G. Souza and R. Saito, *Carbon*, 2002, **40**, 2043-2061.
- 35 20. C. Bussy, K. T. Al-Jamal, J. Boczkowski, S. Lanone, M. Prato, A. Bianco and K. Kostarelos, *ACS Nano*, 2015, **9**,
- 36 7815-7830.
- 37 21. K. Saijo and C. K. Glass, *Nat Rev Immunol*, 2011, **11**, 775-787.
- 38 22. M. Prinz and J. Priller, *Nat Rev Neurosci*, 2014, **15**, 300-312.
- 39 23. J. Saura, J. M. Tusell and J. Serratos, *Glia*, 2003, **44**, 183-189.
- 40 24. V. E. Kagan, A. A. Kapralov, C. M. St Croix, S. C. Watkins, E. R. Kisin, G. P. Kotchey, K. Balasubramanian, I. I.
- 41 Vlasova, J. Yu, K. Kim, W. Seo, R. K. Mallampalli, A. Star and A. A. Shvedova, *ACS Nano*, 2014, **8**, 5610-5621.
- 42 25. J. Russier, C. Menard-Moyon, E. Venturelli, E. Gravel, G. Marcolongo, M. Meneghetti, E. Doris and A. Bianco,
- 43 *Nanoscale*, 2011, **3**, 893-896.
- 44 26. X. Liu, R. H. Hurt and A. B. Kane, *Carbon N Y*, 2010, **48**, 1961-1969.
- 45 27. G. P. Kotchey, B. L. Allen, H. Vedala, N. Yanamala, A. A. Kapralov, Y. Y. Tyurina, J. Klein-Seetharaman, V. E.
- 46 Kagan and A. Star, *ACS Nano*, 2011, **5**, 2098-2108.
- 47 28. G. P. Kotchey, Y. Zhao, V. E. Kagan and A. Star, *Adv Drug Deliv Rev*, 2013, **65**, 1921-1932.
- 48 29. C. F. Chiu, B. A. Barth, G. P. Kotchey, Y. Zhao, K. A. Gogick, W. A. Saidi, S. Petoud and A. Star, *J Am Chem Soc*,
- 49 2013, **135**, 13356-13364.
- 50 30. V. Neves, E. Heister, S. Costa, C. Tilmaciu, E. Borowiak-Palen, C. E. Giusca, E. Flahaut, B. Soula, H. M. Coley, J.
- 51 McFadden and S. R. P. Silva, *Adv Funct Mater*, 2010, **20**, 3272-3279.
- 52 31. Y. Sato, A. Yokoyama, Y. Nodasaka, T. Kohgo, K. Motomiya, H. Matsumoto, E. Nakazawa, T. Numata, M. Zhang,
- 53 M. Yudasaka, H. Hara, R. Araki, O. Tsukamoto, H. Saito, T. Kamino, F. Watari and K. Tohji, *Sci Rep*, 2013, **3**,
- 54 2516.
- 55 32. V. E. Kagan, N. V. Konduru, W. Feng, B. L. Allen, J. Conroy, Y. Volkov, Vlasova, II, N. A. Belikova, N. Yanamala, A.
- 56 Kapralov, Y. Y. Tyurina, J. Shi, E. R. Kisin, A. R. Murray, J. Franks, D. Stolz, P. Gou, J. Klein-Seetharaman, B.
- 57 Fadeel, A. Star and A. A. Shvedova, *Nat Nanotechnol*, 2010, **5**, 354-359.
- 58 33. A. Bianco, K. Kostarelos and M. Prato, *Chem Commun (Camb)*, 2011, **47**, 10182-10188.
- 59 34. B. L. Allen, P. D. Kichambare, P. Gou, Vlasova, II, A. A. Kapralov, N. Konduru, V. E. Kagan and A. Star, *Nano Lett*,
- 60 2008, **8**, 3899-3903.
- 61 35. R. Kurapati, J. Russier, M. A. Squillaci, E. Treossi, C. Menard-Moyon, A. E. Del Rio-Castillo, E. Vazquez, P.
- 62 Samori, V. Palermo and A. Bianco, *Small*, 2015, **11**, 3985-3994.

- 1 36. F. T. Andon, A. A. Kapralov, N. Yanamala, W. Feng, A. Baygan, B. J. Chambers, K. Hultenby, F. Ye, M. S. Toprak,  
2 B. D. Brandner, A. Fornara, J. Klein-Seetharaman, G. P. Kotchey, A. Star, A. A. Shvedova, B. Fadeel and V. E.  
3 Kagan, *Small*, 2013, **9**, 2721-2729, 2720.
- 4 37. A. A. Shvedova, A. A. Kapralov, W. H. Feng, E. R. Kisin, A. R. Murray, R. R. Mercer, C. M. St Croix, M. A. Lang, S.  
5 C. Watkins, N. V. Konduru, B. L. Allen, J. Conroy, G. P. Kotchey, B. M. Mohamed, A. D. Meade, Y. Volkov, A. Star,  
6 B. Fadeel and V. E. Kagan, *PLoS One*, 2012, **7**, e30923.
- 7 38. C. M. Girish, A. Sasidharan, G. S. Gowd, S. Nair and M. Koyakutty, *Adv Healthc Mater*, 2013, **2**, 1489-1500.
- 8 39. L. C. Davies, S. J. Jenkins, J. E. Allen and P. R. Taylor, *Nat Immunol*, 2013, **14**, 986-995.
- 9 40. S. Lanone, P. Andujar, A. Kermanizadeh and J. Boczkowski, *Adv Drug Deliv Rev*, 2013, **65**, 2063-2069.
- 10 41. H. Nagai, Y. Okazaki, S. H. Chew, N. Misawa, Y. Yamashita, S. Akatsuka, T. Ishihara, K. Yamashita, Y. Yoshikawa,  
11 H. Yasui, L. Jiang, H. Ohara, T. Takahashi, G. Ichihara, K. Kostarelos, Y. Miyata, H. Shinohara and S. Toyokuni,  
12 *Proc Natl Acad Sci U S A*, 2011, **108**, E1330-1338.
- 13 42. I. Fenoglio, E. Aldieri, E. Gazzano, F. Cesano, M. Colonna, D. Scarano, G. Mazzucco, A. Attanasio, Y. Yakoub, D.  
14 Lison and B. Fubini, *Chem Res Toxicol*, 2012, **25**, 74-82.
- 15 43. M. J. Osmond-McLeod, C. A. Poland, F. Murphy, L. Waddington, H. Morris, S. C. Hawkins, S. Clark, R. Aitken, M.  
16 J. McCall and K. Donaldson, *Part Fibre Toxicol*, 2011, **8**, 15.
- 17 44. Vlasova, I., T. V. Vakhrusheva, A. V. Sokolov, V. A. Kostevich, A. A. Gusev, S. A. Gusev, V. I. Melnikova and A. S.  
18 Lobach, *Toxicol Appl Pharmacol*, 2012, **264**, 131-142.
- 19 45. H. Ali-Boucetta, K. T. Al-Jamal, K. H. Muller, S. Li, A. E. Porter, A. Eddaoudi, M. Prato, A. Bianco and K. Kostarelos,  
20 *Small*, 2011, **7**, 3230-3238.
- 21 46. K. T. Al-Jamal, H. Nerl, K. H. Muller, H. Ali-Boucetta, S. Li, P. D. Haynes, J. R. Jinschek, M. Prato, A. Bianco, K.  
22 Kostarelos and A. E. Porter, *Nanoscale*, 2011, **3**, 2627-2635.
- 23 47. T. Fath, Y. D. Ke, P. Gunning, J. Gotz and L. M. Ittner, *Nat Protoc*, 2009, **4**, 78-85.
- 24 48. M. Ni and M. Aschner, *Curr Protoc Toxicol*, 2010, **Chapter 12**, Unit 12 17.
- 25 49. M. S. Dresselhaus, G. Dresselhaus, R. Saito and A. Jorio, *Physics Reports*, 2005, **409**, 47-99.
- 26 50. M. S. Dresselhaus, A. Jorio, M. Hofmann, G. Dresselhaus and R. Saito, *Nano Lett*, 2010, **10**, 751-758.
- 27 51. A. Cuesta, P. Dhamelincourt, J. Laureyns, A. Martinezalonso and J. M. D. Tascon, *Carbon*, 1994, **32**, 1523-1532.
- 28  
29  
30  
31  
32

## Figure Legends

**Figure 1: Characteristics of the different types of functionalized MWNTs.** (a) Chemical structures of the different chemically functionalized MWNTs; (b) Table providing the abbreviations used in the manuscript, the length and the amount of amino groups for the different MWNTs; (c) Raman spectra were collected on the starting MWNT suspension before cell exposure. Three characteristic bands are observed: D band at  $\sim 1330\text{ cm}^{-1}$ , G band at  $\sim 1585\text{ cm}^{-1}$ , and D' band at  $\sim 1620\text{ cm}^{-1}$ . A clearer D' band was observed for both carboxylated MWNTs, ox-MWNT and ox-MWNT-NH<sub>3</sub><sup>+</sup>, in comparison to MWNT-NH<sub>3</sub><sup>+</sup>.

**Figure 2: Live imaging of primary microglia exposed to different functionalized MWNTs via optical microscopy.** Primary microglia enriched cell cultures were exposed during 24 h to a unique dose of different MWNTs (10  $\mu\text{g/mL}$ ) and then leaved for different period of time before imaging. (a) Schematic of the study design providing the different recovery times after the single exposure to MWNTs. (b) Microglia at day 1 to 90. No significant difference in terms of shape or number of cells was observed between the non-exposed cells and the cells exposed to MWNTs at any time of recovery after the initial exposure. Scale bar = 50  $\mu\text{m}$ .

**Figure 3: Optical microscopy of single primary microglial cell before Raman spectroscopy.** Primary microglia cultures were fixed with pre-cooled methanol at the end of each desired time and then air dried for at least one hour before further analysis. Representative pictures of single cells observed with a 100x objective in bright field illumination are provided for each exposure and time points, together with numbers showing the typical positions where Raman spectra were collected. No significant difference was observed between the different MWNT exposures. For each cell analysed via Raman spectroscopy, three regions could be distinguished: a clear region in the centre of the cell corresponding to the nuclear area where no CNT Raman scattering can be detected, a darker region surrounding the nucleus and attributed to the intracellular accumulation of MWNTs because of the Raman scattering collected, and another clear region delimitating the cell boundaries or extremities where no CNT Raman scattering can be detected. Scale bar = 10  $\mu\text{m}$ .

**Figure 4: Raman spectroscopy of microglia cell culture monolayer after exposure to different f-MWNTs.** Following the collection of a Raman spectrum, the intensity ratio between D and G bands was calculated from normalised intensity of D and G bands for each spectrum. Intensities were normalised to the intensity of G band ( $I_G = 1$ ). The intensity  $I_D/I_G$  band ratio for all spectra collected (a, c, e) and the average  $I_D/I_G$  band ratio (b, d, f) are presented for microglia expose to ox-MWNT (a, b), ox-MWNT-NH<sub>3</sub><sup>+</sup> (c, d) and to MWNT-NH<sub>3</sub><sup>+</sup> (e, f). An overall continuous decrease of  $I_D/I_G$  band ratio was observed over time, more significant during the first 14 days for both oxidised materials compared to aminated MWNTs. Between 12 and 22 spectra were collected and analysed for each sample.

**Figure 5: Raman spectroscopy of MWNT-NH<sub>3</sub><sup>+</sup>.** For some Raman spectra collected in primary microglia exposed to MWNT-NH<sub>3</sub><sup>+</sup> at late time points (30, 60, 90 days), we observed a distinct D' band next to the G band, in contrast to the starting MWNT-NH<sub>3</sub><sup>+</sup> material in which this D' band was absent. A representative spectrum of this phenomenon is provided for MWNT-NH<sub>3</sub><sup>+</sup> exposed microglia analysed at 90 day time point.

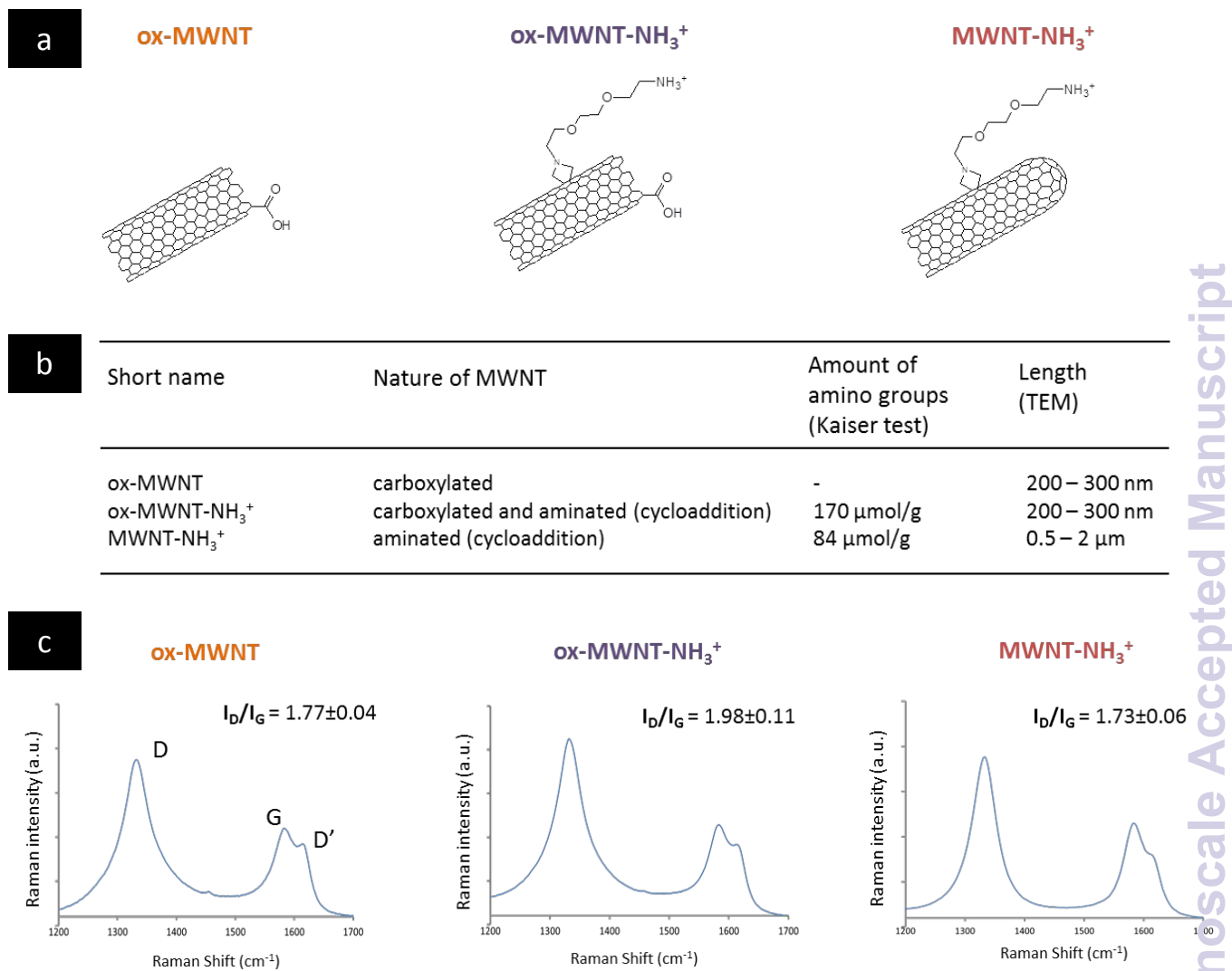
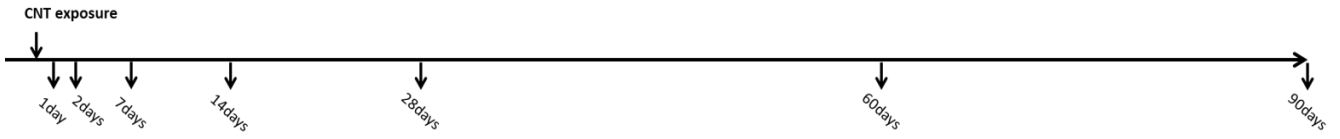
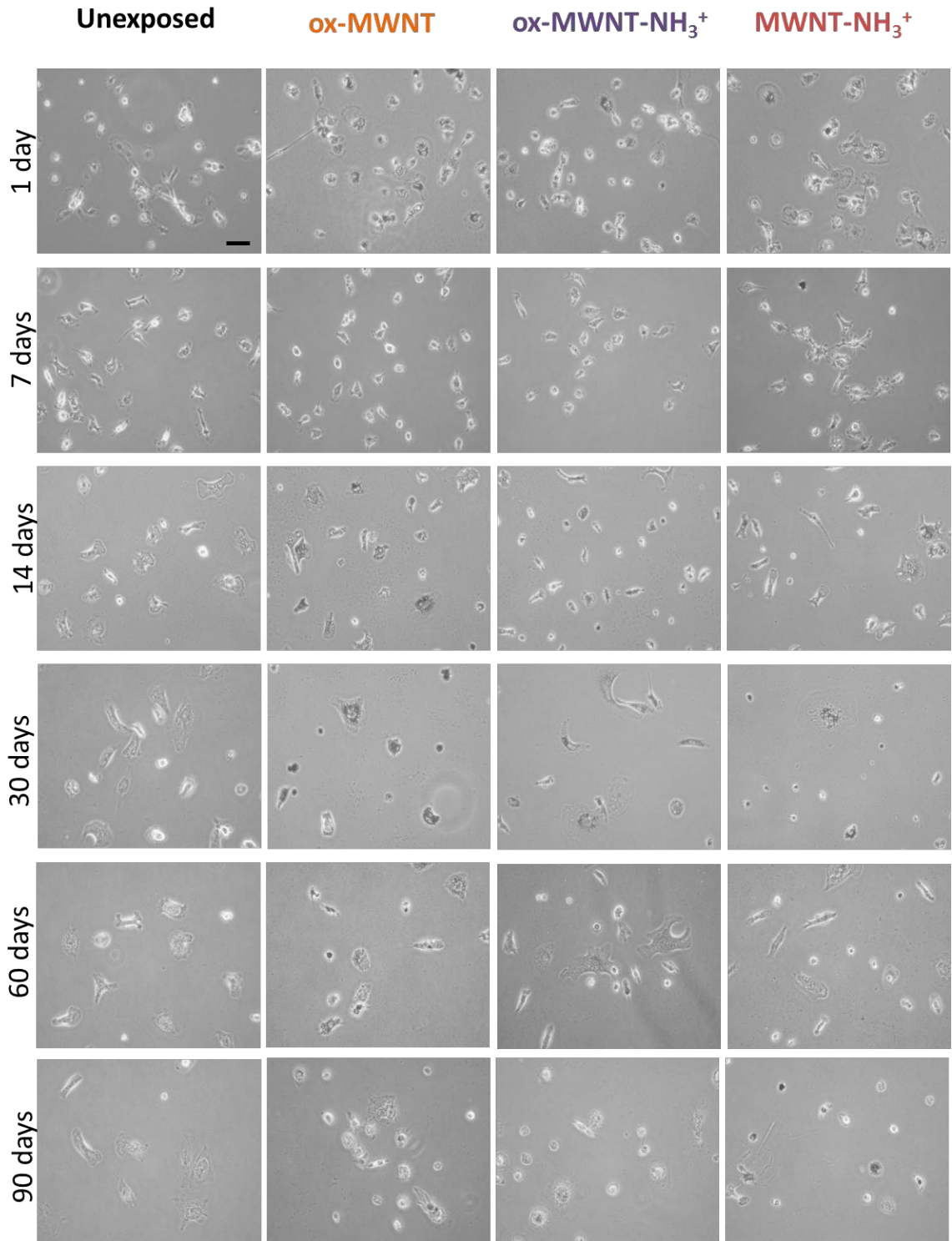


Figure 1

a



b



Nanoscale Accepted Manuscript

Figure 2

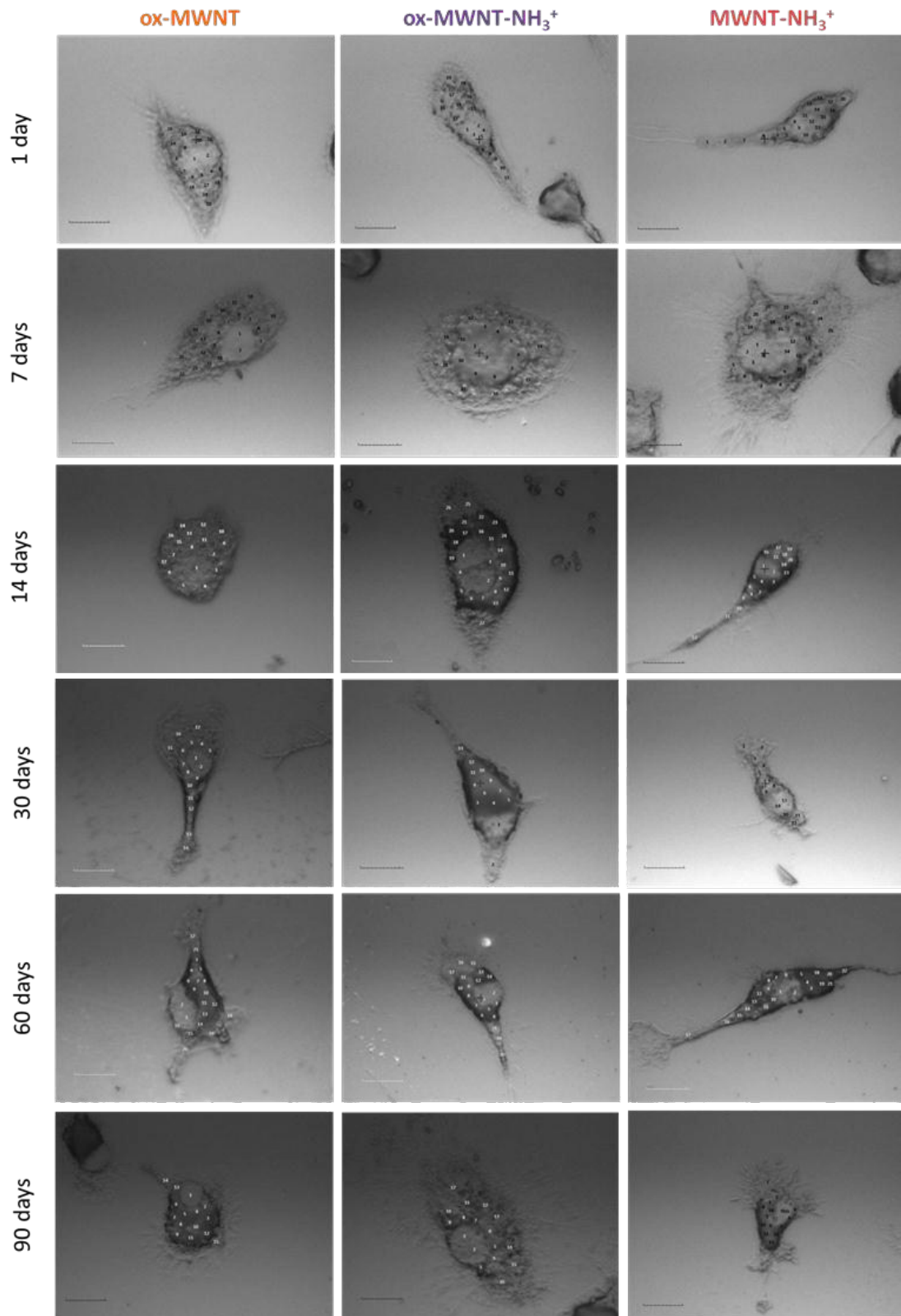


Figure 3

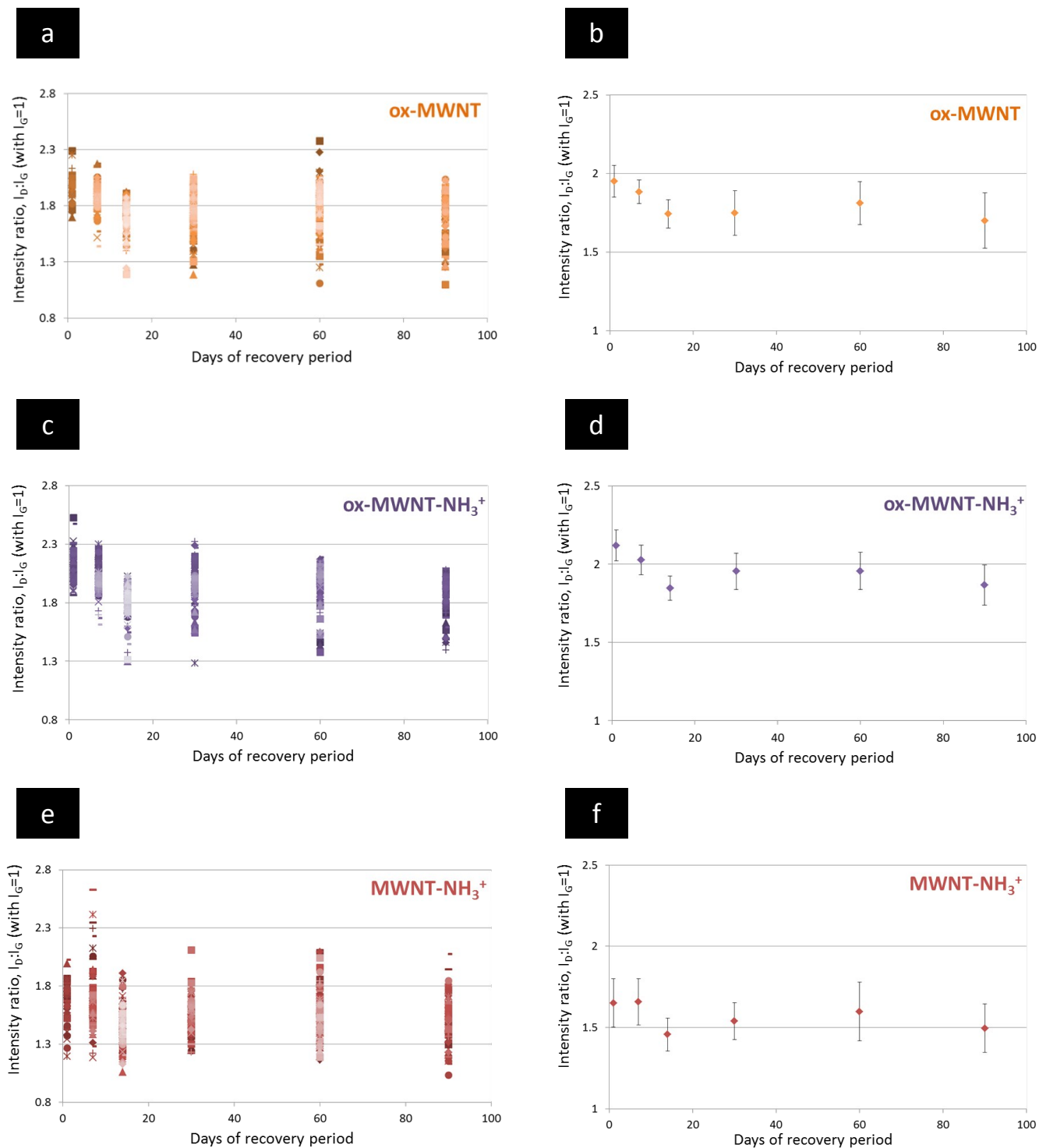


Figure 4

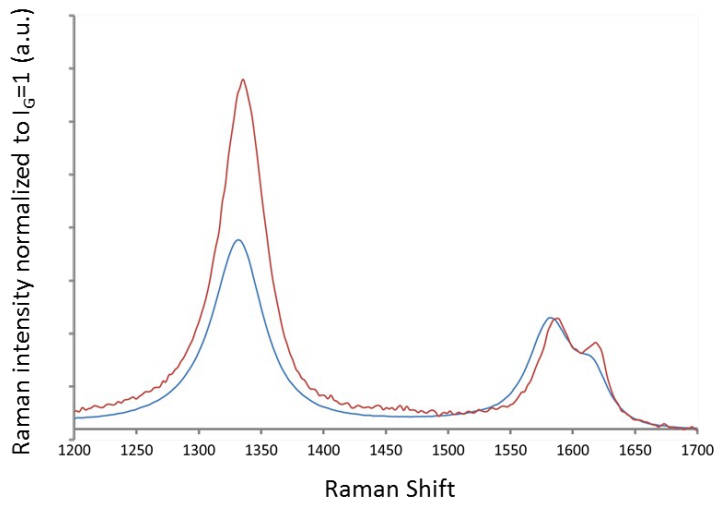


Figure 5